THE FLOW OVER ASYMMETRICAL RIPPLES: AN EXPERIMENTAL INVESTIGATION ON THE MORPHODYNAMIC BEHAVIOR

Carla Faraci[1], Carmelo Petrotta[2], Pietro Scandura[3], Enrico Foti[4] and Paolo Blondeaux[5]

This paper reports on an experimental campaign focused on the generation and evolution of small scale bedforms over a sloping sandy beach. The wave propagation over a sloping bed triggers a flow asymmetry that reflects on the bedform characteristics. Morphodynamic analyses on ripple evolution and migration led to observe that at the equilibrium the ripples have larger offshore flanks and are leant toward the beach. However migration velocity may be onshore or offshore directed. The equilibrium ripple characteristics seem to be well described by Nielsen (1981) ripple predictor.

Keywords: ripple evolution; asymmetric waves; migration velocity

INTRODUCTION

In a coastal environment, waves and currents propagating over a non cohesive sandy bottom often trigger the appearance of small scale sedimentary structures. Such bedforms, known as ripples, induce a considerable modification of the bed roughness and, in turn, affect the hydrodynamics inside the boundary layer at a large extent.

Sea ripples have been deeply studied both theoretically and experimentally (see, for example, Sleath, 1984, Nielsen, 1992, Blondeaux, 2001). Several authors performed a large number of laboratory investigations on ripple geometry in order to propose ripple predictor models based on the flow parameters (e.g. Nielsen 1981; Mogridge et al., 1994; Wiberg & Harris, 1994, Faraci and Foti 2002, Grasmeijer and Kleinhans, 2004, Camenen 2009), applicable to equilibrium conditions. Doucette and O'Donoghue (2006) investigated at full scale conditions the effects of flow changes on ripple characteristics. Blondeaux et al. (2000) found that because of the presence of a steady velocity component in the direction of wave propagation, ripples migrate at a constant rate which is predicted as function of sediment and wave characteristics.

In the field, the ripples characteristics are affected by the wave shape which is subject to important variations during propagation from deep to shallow waters. At intermediate depth, because of nonlinearities, the crests become sharp and the through flatter and wider, thus giving rise to skewed waves. When the waves enter in the shallow water region they also become asymmetric, with a steep front and a moderate sloping rear side. Both skewed and asymmetric waves strongly affect the hydrodynamics within the bottom boundary layer and in turn even the bed-form characteristics. More specifically, under skewed or asymmetric waves the peak of the velocity oscillation in the onshore half-cycle is larger than that occurring during the offshore half-cycle. Therefore this asymmetry induces the appearance of asymmetric ripples and a preferential direction in the sediment transport.

These phenomena were investigated for skewed waves by Sato & Horikawa (1986) who showed the ripples are asymmetric under skewed oscillatory flows with the onshore flank of the ripples steeper than the offshore one. Measurements in an oscillatory flow over sand ripples were carried out by vand der Werf et al. (2007) in a water tunnel. They reported that the asymmetry of the oscillatory flow produces steady circulation cells with a dominant offshore mean flow.

Hurther & Thorne (2011) measured in a large-scale wave flume the effect of wave skewness on ripples vortex entrainment and sediment transport. They reported that the net onshore transport of sediments is the cause of the onshore ripple migration.

Recently Scandura et al. (2016) reported that in the boundary layer at the bottom of asymmetric waves the period-averaged Reynolds stress does not vanish, thus triggering an offshore directed steady streaming which persists into the irrotational region.

The asymmetry of both flow and ripples is considered to be strongly related to the direction and the net rate of sediment transport.

[1] Department of Engineering, University of Messina, C.da di Dio, S. Agata 98166 Messina, Italy.
[2] Department of Engineering, University of Messina, C.da di Dio, S. Agata 98166 Messina, Italy.
[3] Department of Civil Engineering and Architecture, University of Catania, v.le A. Doria 6, 95125 Catania, Italy.
[4] Department of Civil Engineering and Architecture, University of Catania, v.le A. Doria 6, 95125 Catania, Italy.
[5] Department of Civil Chemical and Environmental Engineering, University of Genova, via Montallegro 1, 16145 Genova, Italy.

Even though there is a large number of literature studies on ripple formation and evolution on horizontal bottom and a few studies on asymmetric and skewed waves propagating over a sandy bottom, to the authors' knowledge no attention has been devoted to the case of waves propagating on a sandy sloping bed.

The present paper reports some preliminary results of an experimental campaign focused on the investigation of ripples generated by regular and random waves propagating over a sloping sandy beach. The asymmetry of the flow is induced by the sloping bed and is thus reflected on the generated bedforms.

The paper is organized as follows: the next section describes the experimental set up and procedure. Then, the experimental results, divided in two subsections one for the bedform evolution and another for the equilibrium conditions, are discussed. Finally the paper ends with some conclusions.

EXPERIMENTAL SET UP AND PROCEDURE

The experimental campaign which focused on the interaction between asymmetrical oscillatory flows and rippled beds, was performed in the hydraulics laboratory of the University of Messina (Italy). Experiments were carried out in a wave flume 18.5 m long, 0.4 m wide and 0.8 m high with flat stainless steel bottom and glass walls (Figure 1a).

Waves are generated within the flume by means of a flap type wavemaker which is able to reproduce both regular and random waves characterized by wave heights up to 0.12 m and wave periods between 0.5 and 2 s. The wavemaker was driven by a pneumatic system and was electronically controlled. In the present campaign both regular and random waves were generated. Regular waves were generated using a panel to set the signal frequency, amplitude and offset position, while the random waves were generated using a software that reproduces a TMA spectrum with a peak enhancement factor of 3.3. For random waves, a time series of 180 sec was generated and identically repeated during the experiments.

At the back of the wavemaker some mattresses of creased pipe pieces were placed to absorb any spurious reflection caused by the flap. More details on the experimental setup can be found in Liu and Faraci (2014) and Faraci et al. (2015).

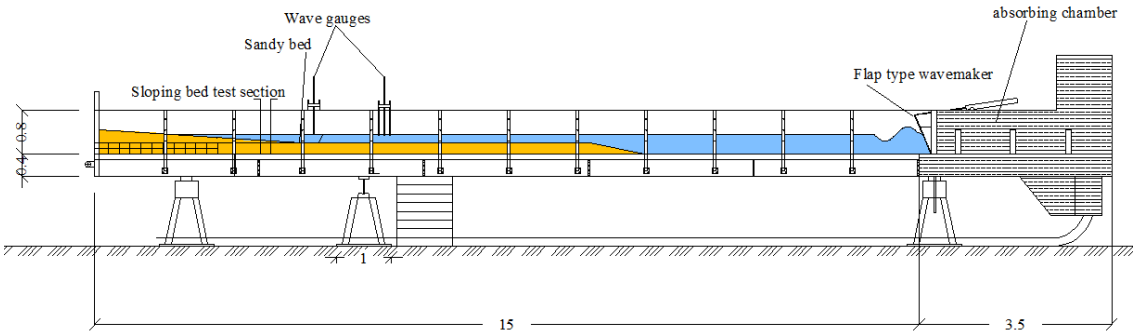

(a)

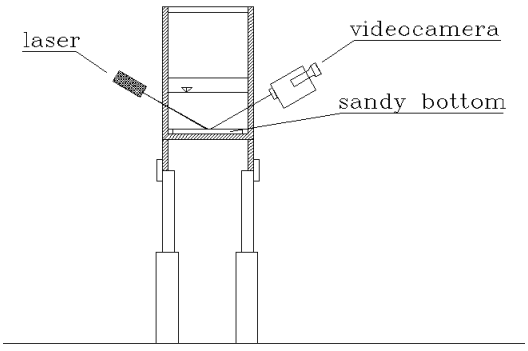

(b)

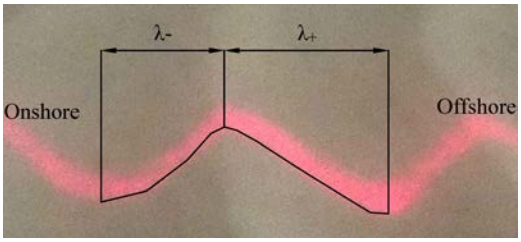

(c)

Figure 1. Experimental set up adopted in the present experimental campaign (a); sketch of the optical structured light technique (b); example of the laser light on the sandy bottom with the two half-wavelength λ+ and λ- (c).

Starting at 8 m away from the wavemaker and for the remaining flume length, the bottom was covered with a layer of 0.2 m thick of uniform sand, characterized by a median grain size d_{50}=0.25 mm. A plane beach, 3.5 m long with a slope of 1: 10, was built oppositely to the wavemaker in order to minimize reflection. Moreover the plane beach had the function to trigger the asymmetry of the waves propagating along the flume.

Regular and random waves characterized by heights between 1 and 10 cm and periods between 0.8 and 1.4 s were generated and propagated along the flume and their effect on the sandy bed was analyzed.

Measurements of wave characteristics throughout the wave flume were performed by means of five resistive level probes. The first one was located 5 m off the wavemaker, three of them were placed on the horizontal sand layer and spaced in such a way to allow the wave reflection along the flume to be evaluated by means of Mansard and Funke's (1980) method. The last one was located on the sloping beach where the waves shoal.

Flow characteristics were acquired by means of a Vectrino Profiler (Nortek As.) with sampling rate equal to 100 Hz and a cell size set equal to 1 – 2 mm.

The bed morphology was acquired by means of a structured light optical system (see Faraci and Foti, 2002 or Faraci et al., 2012 for details on the technique). The light sheet optically slices the measured body creating a cross-sectional image that can be observed and recorded through a video camera and then analyzed to obtain the desired ripple dimensions (Figure 1 b and 1c).

Once the image was gathered by the video camera, suitable image processing procedures was adopted, in particular the correspondence between the image units, given in pixels, and the object dimensions were preliminary stated. This task was accomplished by acquiring the image of a known object and deriving the coefficients which give the unit dimension of one pixel in both horizontal and vertical directions.

Each experiment required some preliminary operations, i.e. the definition of the control parameters to be provided to the wavemaker in order to generate the desired wave, the choice of the Vectrino profiler software configuration, the calibration of the optical system, the leveling of the sandy bed. This last task had to be carefully performed in order to remove any ripple mark from the sandy bed and to start each experiment from an initially flat condition.

Hydrodynamic and morphodynamic measurements had to be acquired separately. Indeed the flow measurements required enough suspension in order to allow the acoustic signal to be reflected by the suspended particles. The morphodynamic measurements instead had to be performed in perfectly clear water to make the image formation possible on the camcorder lenses. Thus the experimental procedure followed such a schedule:

- In the presence of clear water and starting from an initially flat bed, the waves propagated on the sandy bottom and triggered the formation of ripple bedforms. In the same time the structured light approach was used to acquire the rippled bed images by means of a camera. The morphodynamic acquisition ended once the equilibrium was achieved, which generally occurred within 15 minutes.
- Once the morphodynamic measurements were performed, the water was seeded by means of talc powder and two vertical profiles were acquired, the first one located on the horizontal sandy bottom, the other one on the sloping bed.

A post-processing stage was then performed in order to interpret the acquired images according to the optical technique with the aim of determining their dimensions.

ANALYSIS OF THE RESULTS

Experiments

Thirteen experiments were performed. Ten of these experiments were carried out in the presence of regular waves, and three in the presence of random waves. In Table 1 the experimental parameters of each test are reported; the last three rows refer to random waves. In particular the first column indicates the test name, then the second column reports the water depth and the last two columns the wave height (or the significant wave height in the case of random waves) and the period (or mean period in the case of random waves). It is worth pointing out that the water depth is measured on the sloping bottom at the cross section where ripple characteristics are measured.

Table 1. Hydraulic characteristics of the performed experiments				
Test name		d [m]	H_m, H_s [m]	T_m [s]
R	CF_1	0.1450	0.0675	1.2324
E	DT_7	0.1450	0.0694	1.2183
G	DT_5	0.1450	0.0713	1.0100
	DT_4	0.1450	0.0825	1.0100
W	AB_4	0.1450	0.1006	1.0101
A	DT_1	0.1450	0.0573	0.8412
V	LM_1	0.1450	0.0958	0.8402
E	LM_2	0.1450	0.0911	0.8400
S	DT_3	0.1470	0.1270	0.8399
	AB_8	0.1450	0.1217	0.8400
R	LC_1	0.1360	0.0797	0.9149
A	LC_2	0.1380	0.0630	0.8041
N	LC_3	0.1340	0.0588	0.9113

In Figure 2 an example of the water elevation, as recorded by the onshore located wave gauge, is reported for the two regular wave tests named DT_3 and DT_4.

The dimensionless parameters usually employed in the analysis of ripple dynamics are:

- the relative density of sediments:

$$s = \frac{\rho_s}{\rho} \tag{1}$$

- the flow Reynolds number:

$$\mathrm{Re} = \frac{U_0 A}{\nu} \tag{2}$$

- the sediment Reynolds number:

$$\mathrm{Re}_d = \frac{U_0 d_{50}}{\nu} \tag{3}$$

- the mobility number:

$$\psi = \frac{{U_0}^2}{(s-1) g d_{50}} \tag{4}$$

- the Shields parameter (related to the mobility number):

$$\vartheta_{2.5} = \frac{1}{2} f_w \frac{{U_0}^2}{(s-1) g d_{50}} \tag{5}$$

Where:

- ρ_s is the sediment density;
- ρ is the water density;
- U_0 is the orbital velocity;
- A is the orbital amplitude;
- ν is the kinematic water viscosity;
- d_{50} is the median grain size;
- f_w is the friction factor defined in terms of Re and A/d_{50}.

In the following subsections the morphodynamic behavior of the rippled bed is analyzed in terms of bedform evolution and their characteristics at the equilibrium.

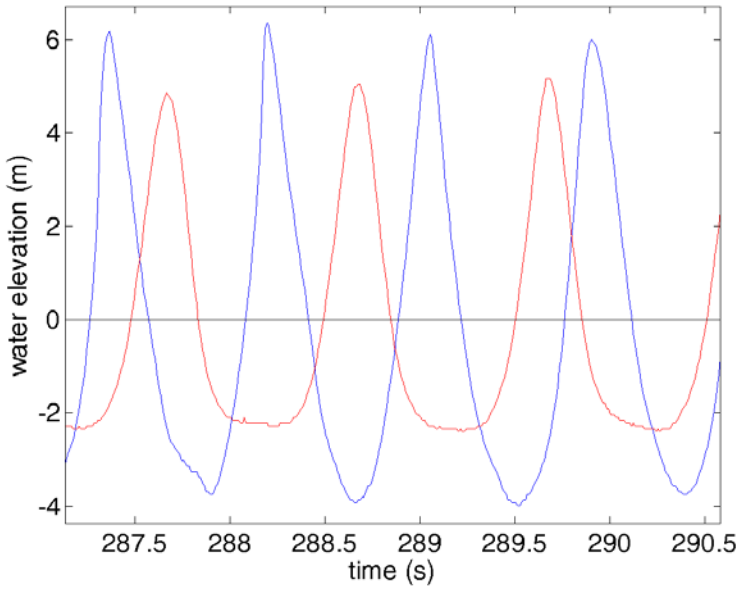

Figure 2. An example of the water elevation for two regular wave tests (blue line: test DT_3: H=0.12 m; T=0.84 s; red line: test DT_4: H=0.082 m; T=1.00 s).

Experimental results

In the present paper, the morphodynamic characteristics of a rippled bed generated by waves propagating over a sloping sandy bed are analyzed. As previously mentioned, also the hydrodynamic characteristics of the flow were measured but they will be discussed in an upcoming paper.

In Table 2 the ripple characteristics at the equilibrium, namely the ripple wavelength λ, the ripple height η and their velocity of migration v_o are reported for each test. Table 2 also reports the main dimensionless parameters previously mentioned. In particular, the last three columns indicate the flow Reynolds number, the sediment Reynolds number and the mobility number respectively. The sediment relative density was constant and equal to s=2.65 throughout the experimental campaign, thus it is not included in the table.

Table 2. Morphodynamic characteristics of the performed experiments

Test name	λ [m]	η [m]	v_o [cm·min^{-1}]	Re	Re_d	ψ
CF_1	0.0607	0.0148	0.0375	5388.8560	45.7716	8.2870
DT_7	0.0526	0.0096	0.1133	5173.2583	49.1782	9.5664
DT_5	0.0528	0.0088	0.0012	4537.8682	46.0619	8.3924
DT_4	0.0571	0.0086	-0.2118	6357.4961	54.5172	11.7563
AB_4	0.0617	0.0073	-0.1321	31333.6701	99.9217	39.4933
DT_1	0.0334	0.0043	-0.1521	2153.8072	31.7091	3.9771
LM_1	0.0393	0.0076	-0.0814	3682.2533	37.8378	5.6631
LM_2	0.0434	0.0074	-0.6836	5504.2975	46.2616	8.4653
DT_3	0.0527	0.0070	-0.4050	6179.0165	53.7401	11.4235
AB_8	0.0400	0.0060	-0.0435	7490.7005	49.1376	9.5506
LC_1	0.0569	0.0088	0.0018	5580.7899	48.9430	9.4751
LC_2	0.0433	0.0068	-0.0409	2862.7271	37.3908	5.5301
LC_3	0.0519	0.0086	0.0056	3148.2308	36.8326	5.3662

Bedform evolution

Ripple marks appear after the propagation of few tens of waves on the sandy bed. They appear almost simultaneously on the horizontal bed and on the slope. In Figure 3 the evolution of ripple wavelength and height is shown for the regular wave test DT_3 (H=0.12 m; T=0.83 s). Both these quantities are obtained by averaging over three different ripples which fall within the acquired image.

The wavelength assumes an initial value which is about two thirds of the final equilibrium value. Then, it increases almost linearly for the first 11 minutes and after that it reaches an almost constant value which is maintained until the end of the test.

The ripple height increases with an asymptotic law and reaches the equilibrium at the very beginning of the experiment, i.e. after the first 3-4 minutes. Then, it maintains a constant value for all the test duration. The test was run for fifteen minutes since after such time interval no appreciable variation of the measured quantities were observed.

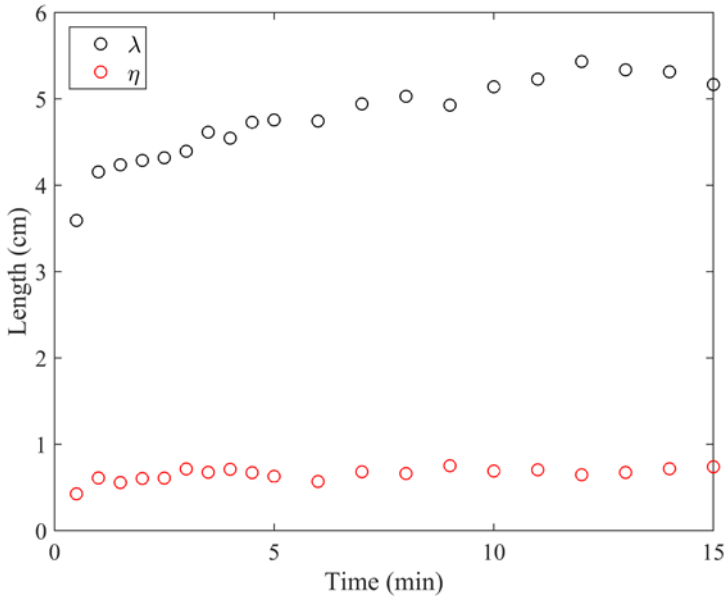

Figure 3. Ripple wavelength and height evolution in the case of regular waves (test DT_3: H=0.12 m; T=0.83 s).

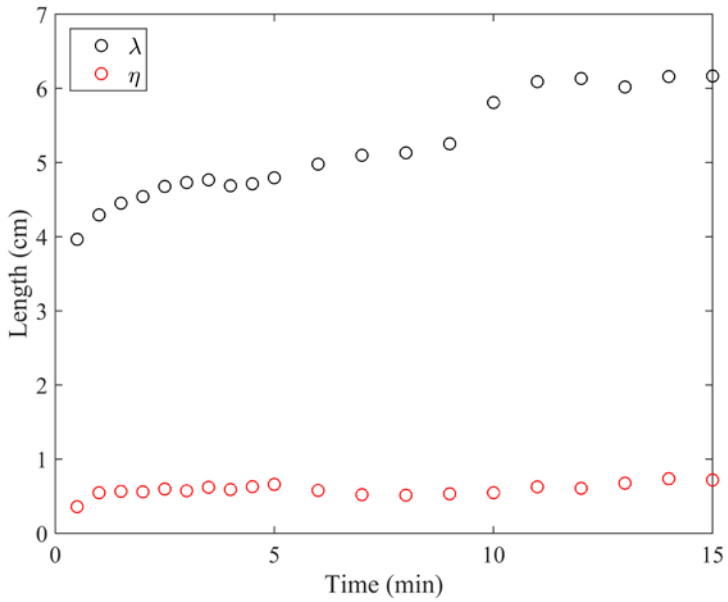

Figure 4. Ripple wavelength and height evolution in the case of random waves (test LC_1: H_s=0.12 m; T=0.93 s).

A similar behavior concerning the evolution of both height and wavelength was observed in the other tests. In few cases a slight jump is observed in the wavelength evolution, corresponding to the fusion or separation of two adjacent ripples. Such jump is however compensated for in a couple of minutes. For example in Figure 4 the evolution of ripple height and wavelength in one of the random

wave tests (LC_1: H_s=0.12 m and T=0.93 s) is shown, and very similar features with respect to the discussed regular wave test can be observed.

In Figure 5 the time evolution of the two half-wavelengths λ+ and λ-, defined according to the sketch plotted in Figure 1c are plotted for the regular test case DT_3. At the beginning of the test the two half-wavelengths are dissimilar, with the offshore half-length λ+ higher than the onshore one λ-. Such a difference between the two half wavelength increases during the test, indicating the generation of a strong asymmetry in the ripples as shown in figure 1c.

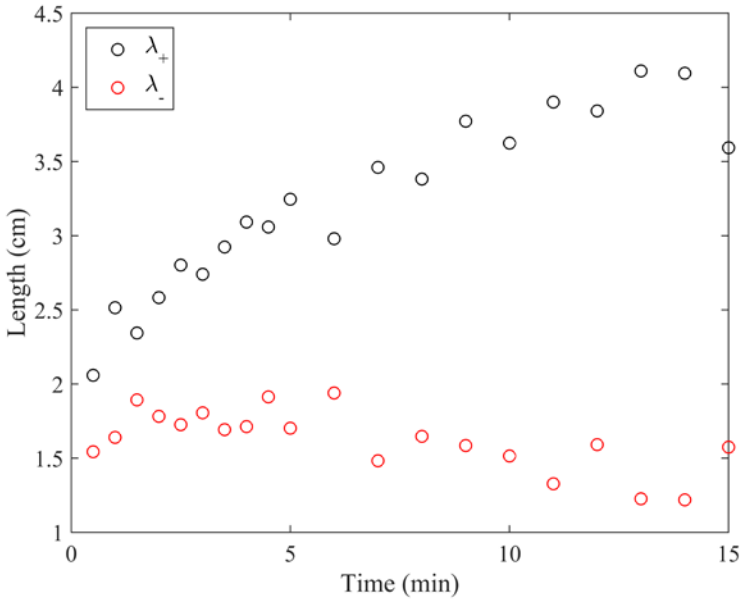

Figure 5. Ripple half-wavelength evolution in the case of regular waves (test DT_3: H=0.12 m; T=0.83 s) See sketch in Figure 1c.

In Figure 6 the time evolution of the migration velocity is plotted for the same test case. It is interesting to note that at the beginning of the experiment and for the first minutes of run, the migration velocity assumes a positive value, i.e. it is onshore directed. After about 3-4 minutes from the beginning of the test the migration changes sign and ripples start to migrate offshore. From the plot in Figure 6, it seems that the bedform migration rate in the offshore direction slightly increases with time and perhaps it will converge to a constant but not vanishing value.

This trend of the migration velocity is the most common behavior in all the experiments. However there are a few cases characterized by ripples which migrate offshore since the beginning of the run. An example is shown in Figure 7, referred to the test case DT_4 (H=0.08 m; T=1.00 s). Here the negative migration velocity overall tends to decrease already since the beginning of the test. The offshore migration rate asymptotically decreases with time tending to zero, i.e. the bedforms tend to reach an equilibrium position. In Figure 8 the migration velocity is shown for the case of random waves: in this case the migration rate is positive but it decreases towards zero.

In an attempt to explain the differences among the data shown in figures 6, 7 and 8, let us recall that the hydrodynamic phenomena that can affect the migration velocity are: the asymmetry of the velocity oscillations close to the bed due to asymmetric and/or skewed waves, the onshore or offshore streaming due to the flow non-linearities, the offshore directed flow (undertow) which balances the onshore flux of water generated between the through and the crest of the wave.

The experiments of van der Werf et al. (2007), carried out in a U-tube, the near bed oscillating flow was similar to that generated at the bottom of a skewed wave and it was observed that ripples migrate onshore. The authors also reported that the net time-averaged suspended sand flux was in the offshore direction while the bed-load transport was in the onshore direction.

The total net transport was in the offshore direction. The near bed streaming can be onshore or offshore, depending on the flow parameters and on the asymmetry of the ripple geometry. It is likely

that, net of other effects, the ripples migrate in the direction of the mean velocity, but in general this is not guaranteed for underwater bedforms subject to oscillating flows. For example, sand waves mostly migrate in the direction of the mean flow, but cases in which the opposite occurs have been reported in literature. Antidunes in rivers represent another case in which the migration is upstream even though in this particular case the flow is steady.

In the present case, the migration velocity is affected by the hydrodynamics in a complex way, hence it is rather difficult to explain the origin of the differences among the measurements shown in Figures 6, 7 and 8.

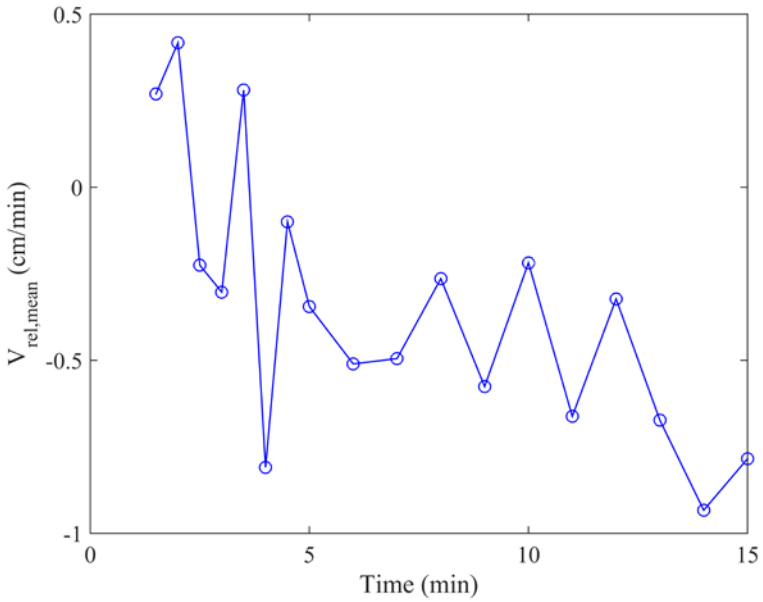

Figure 6. Migration velocity of ripples in the case of regular waves (test DT_3: H=0.12 m; T=0.83 s).

Because of the flow asymmetry, ripples generally migrate onshore. The undertow current, which is proportional to H^2/T, is the largest for the experiment DT_3 (Figure 5). The largest asymmetry of the near bed oscillatory flow is attained for the experiment DT_4 (Figure 7). Then a possible origin for the large offshore migration observed in the experiment DT3 is the larger undertow current along with a small flow asymmetry. In the case of random waves (see Figure 8) even though large variation are observed, it seems that the migration velocity remains close to zero except for a short initial time. Probably this is due to the randomness of the flow filed which does not drive the morphodynamic evolution towards a preferred direction.

Another issue concerns the direction of migration in relation to the ripple asymmetry. In Figure 6 ripples migration is offshore after a sufficient large time has passed, but the steep flank of the ripple is facing onshore (see Figure 5). Even though there are not specific studies for ripples that deal with this issue, for other bedforms such as sand waves there are field observations that show migration in the direction facing the steeper flank. Therefore present results appears rather surprising. In order to provide a reliable explanation of the phenomenon more data would be necessary.

A tentative explanation could be based on the assumption that the steeper onshore flank is due to an onshore bedload transport and the offshore migration is due to an offshore net suspended sand transport, larger in magnitude with respect to the bedload transport, thus an offshore migration is observed. These conditions as concerns the sediment transport have been reported by van der Werf et al. (2007) but the authors did not report information about the ripple asymmetry. Further investigations are planned in order to clarify this aspect.

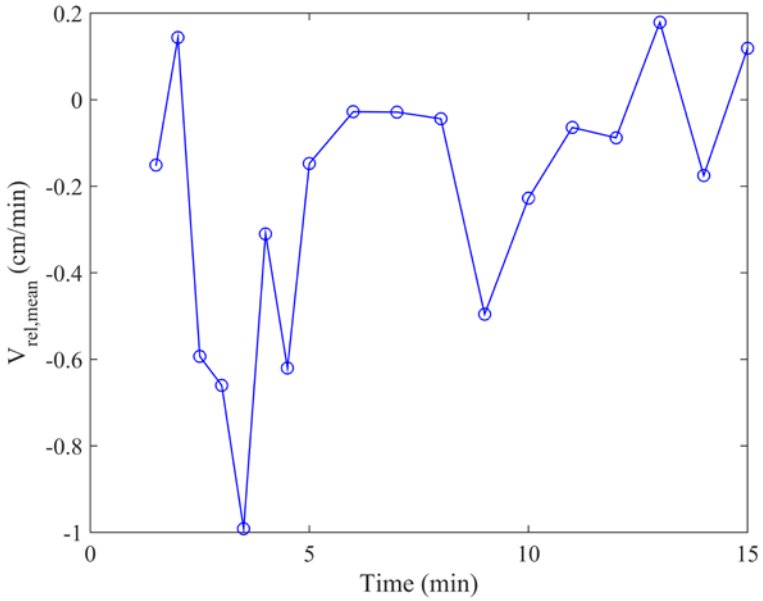

Figure 7. Migration velocity of ripples in the case of regular waves (test DT_4: H=0.08 m; T=1.00 s).

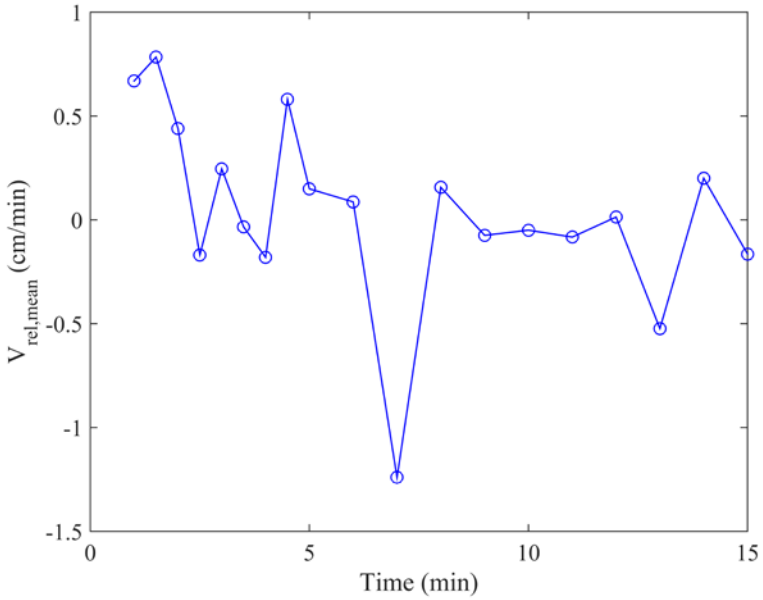

Figure 8. Migration velocity of ripples in the case of random waves (test LC_1: H_s=0.12 m; T=0.93 s).

Equilibrium conditions

The measured equilibrium characteristics of ripples are compared with the results of some predictors, which can be found in literature. More in detail, ripple wavelength, height and steepness at equilibrium are compared with the predictor models of Nielsen (1981), van Rijn (1993) and Grasmeijer and Kleinhans (2004) in Figures 9 to 11.

In particular, in Figure 9 the dimensionless ripple wavelength at the equilibrium is compared with the three mentioned models. The best agreement is with Nielsen's (1981) ripple predictor, both for regular and random waves.

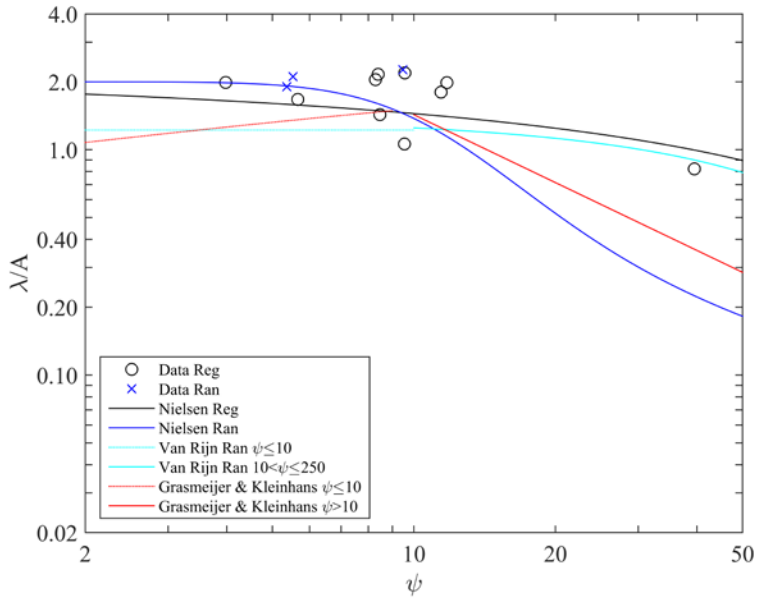

Figure 9. Comparison of non dimensional ripple wavelength data with some ripple predictor models.

The non dimensional ripple height, reported in Figure 10, seems to be underpredicted by all the regular wave ripple predictors. However among the three considered ripple predictors, Nielsen's (1981) predictor is the one which provides the best performances. Nielsen's (1981) predictor for random waves overestimates the ripple height if the mobility number is below 10. A better agreement is provided by van Rijn's (1993) model in the random wave case.

Ripple steepness is well predicted by all the considered models, however regular wave data are better interpreted by Nielsen's (1981) model, while irregular wave data are very well described by the model of Grasmejier and Kleinhans's (2004).

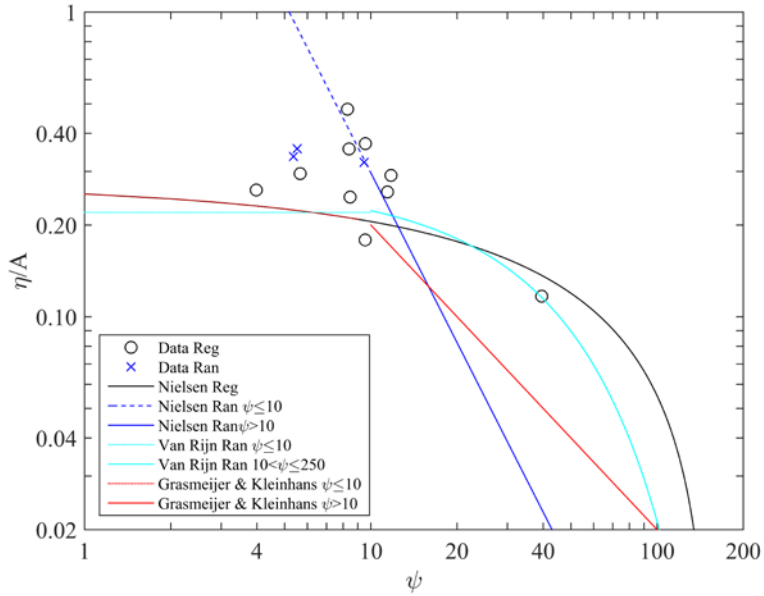

Figure 10. Comparison of non dimensional ripple height data with some ripple predictor models.

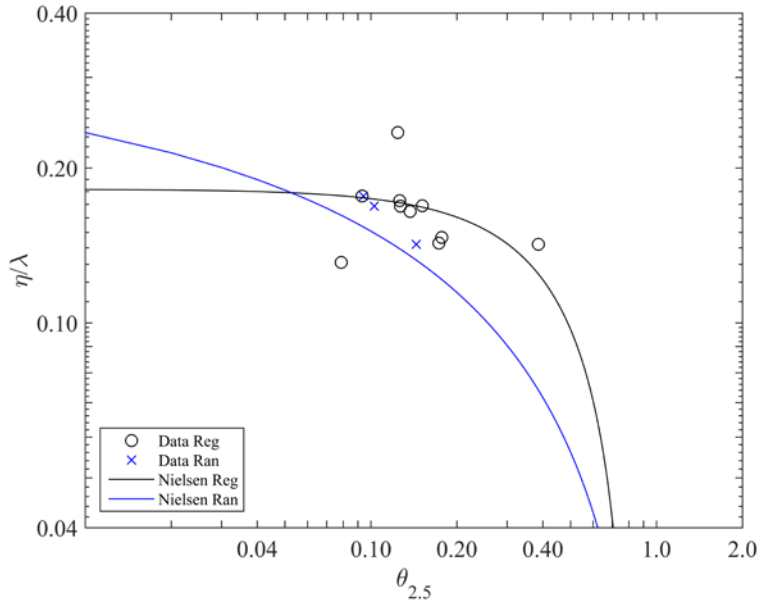

(a)

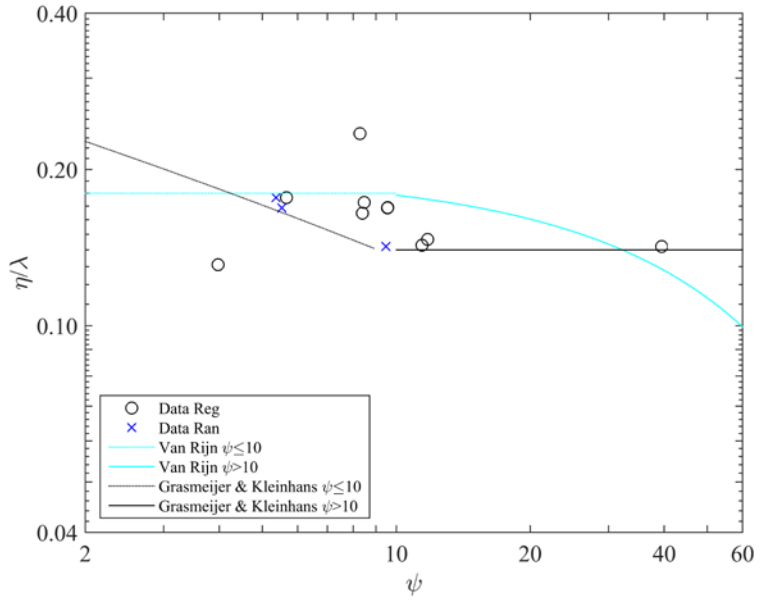

(b)

Figure 11. Comparison of ripple steepness data with some ripple predictor models.

CONCLUSIONS

In this paper the preliminary analyses performed on an experimental campaign aimed at investigating the evolution of sand ripples on a sloping beach under sea waves are described. The morphodynamic evolution of the bed was followed by means of a structured light technique in order to analyze the ripple height, wavelength and migration rate.

It was found that ripples start to appear on the sandy bed as soon as the waves start to interact with the bottom. The bedforms are characterized by a marked asymmetry, with the offshore flank always larger than the onshore one. Contrarily to what would be expected at a first glance, the migration velocity during the time evolution of the ripples often assumes negative values, i.e. bedforms migrate in the offshore direction, even though in most cases when bedforms reach an equilibrium stage, the migration rate tends to zero.

At the equilibrium, ripple characteristics, i.e. height, length and steepness are well interpreted by some of the known ripple predictors, determined for horizontal beds. This leads to assume that the presence of the sloping beach does not play a significant effect on the overall ripple characteristics, while it strongly affects the asymmetry as a consequence of the change in the surface waves which becomes asymmetrical and skewed.

ACKNOWLEDGMENTS

This research has been partially funded by the Italian Ministero dell'Istruzione, dell'Università e della Ricerca through the PRIN 2012 Project 'Hydromorphodynamic modeling of coastal processes for engineering purposes'.

REFERENCES

Blondeaux, P., 2001. Mechanics of coastal forms. *Annu. Rev. Fluid Mech*. 33, 339– 370.

Blondeaux P., Foti E., Vittori G. (2000) Migrating sea ripples. *Eur. J. Mech. B - Fluids* 19, 285–301.

Camenen, B. (2009) Estimation of the wave-related ripple characteristics and induced bed shear stress. Estuarine, *Coastal and Shelf Science*, 84 (4), 553-564.

Doucette, J. S. And O'Donoghue, T. (2006), Response of sand ripples to change in oscillatory flow. *Sedimentology*, 53: 581–596. doi:10.1111/j.1365-3091.2006.00774.x

Faraci, C. and Foti, E. (2002) Geometry, migration and evolution of small-scale bedforms generated by regular and irregular waves. *Coast. Engng*., 47, 35–52.

Faraci, C., Foti, E., Marini A., Scandura, P., (2012). Waves Plus Currents Crossing at a Right Angle: Sandpit Case *J. Waterway, Port, Coast. and Ocean Eng.*, 138(5).

Faraci, C., Scandura, P., and Foti, E. (2015). Reflection of sea waves by combined caissons. *J. Waterway, Port, Coast. and Ocean Eng.*, 141(2).

Grasmeijer, B.T. and Kleinhans, M.G.(2004) Observed and predicted bed forms and their effect on suspended sand concentrations. *Coast. Engng*., 51(5), 351-371.

Hurther D. and Thorne P. (2011) Suspension and near bed load sediment transport processes above a migrating, sand rippled bed under shoaling waves J. Of Geophys. Res., 116, C07001

Liu, Y. and Faraci, C. (2014). Analysis of orthogonal wave reflection by a caisson with open front chamber filled with sloping rubble mound. *Coast. Engng*., 91:151–163.

Mansard, E. P. D., and Funke, E. R. (1980). The measurement of incident and reflected spectra using a least squares method. *Proc., 17th Int. Coastal Engineering Conf.*, ASCE, New York, 154–172.

Mogridge, G.R., Davies, M.H. and Willis, D.H. (1994) Geometry prediction for wave-generated bedforms. *Coast. Engng*., 22, 255–286.

Nielsen, P., 1981. Dynamics and geometry of wave-generated ripples. *J. Geophys. Res.* 86 (C7), 6467–6472.

Nielsen, P., 1992. Coastal bottom boundary layers and sediment transport. World Sci.

Sato, S. and K. Horikawa: Laboratory study on sand transport due to asymmetric oscillatory flows, *Proc. 20th Conf. on Coastal Eng*., pp. 1481-1495, 1986.

Scandura, P., Faraci, C.,and Foti, E. (2016). A numerical investigation of acceleration-skewed oscillatory flows *J. Fluid Mech.* 808, 576-613.

Sleath, J.F.A., 1984. Sea bed mechanics. In: M.E. McCormic (Ed.), *Wiley Ocean Engineering Series*, Wiley, New York.

van der Werf, J. J., Doucette, J. S., O'Donoghue, T., and Ribberink, J. S. (2007): Detailed measurements of velocities and suspended sand concentrations over full-scale ripples in regular oscillatory flow, *J. Geophys. Res.*, 112, F02012

Van Rijn, L.C. (1993) Principles of sediment transport in rivers, estuaries and coastal seas. *Aqua Publications*. Vol. 1006.

Wiberg, P.L. and Harris, C.K. (1994) Ripple geometry in wave-dominated environments. *J. Geophys. Res.*, 99(C1), 775–789.